Development of a Small Punch Test to Evaluate Liquid Metal Embrittlement Susceptibility of 316L Stainless Steel in Liquid Sodium

Stuart Bell[1] (iD), Gaurav Vithalani[1,*] (iD), Richard E. Clegg[1,2] (iD), Geoffrey D. Will[1,3] (iD), Theodore Steinberg[1] (iD), and Rezwanul Haque[3] (iD)

[1]Queensland University of Technology, Australia

[2]Explicom Engineering Investigators, Australia

[3]University of the Sunshine Coast, Australia

*Correspondence: Gaurav Vithalani, gauravlalitbhai.vithalani@hdr.qut.edu.au

Abstract. Liquid sodium is proposed as a heat transfer fluid for solar thermal power receiver designs. It has a long history of use for heat transfer in various industries, with extensive knowledge of its impact on the structural integrity of materials at temperatures ranging from 300 ℃ to 800 ℃. However, the effects at lower temperatures are more poorly understood, which is crucial to studying solar thermal power plant systems. These systems experience diurnal cyclic temperature variation, which causes significant fluctuations in the operating temperature of liquid sodium. Several studies have demonstrated that the susceptibility of metals to Liquid Metal Embrittlement (LME) is highest at temperatures close to the melting point of the liquid metal. Therefore, this study investigates the susceptibility of 316L stainless steel, a common construction material, to sodium induced LME at temperatures between 100 ℃ to 300 ℃ using the Small Punch Test (SPT) method. The test apparatus was validated by using a known embrittling pair of Brass-Galinstan between 10 ℃ to 43 ℃, where the test revealed the expected LME susceptibility of brass. However, no evidence of LME was found in the 316L-sodium pair at temperatures up to 300 ℃.

Keywords: Liquid Sodium, 316L, Liquid Metal Embrittlement (LME)

1. Introduction

The exponential population growth in recent decades has increased the demand for electricity throughout the globe. Considering the impact of traditional electricity production methods on climate change through increased greenhouse gas emissions, electricity generation has been transitioning towards renewable energy sources [1], where Concentrated Solar Power (CSP) plants promise to be a viable alternative due to their capability to generate grid-scale energy with the possibility of achieving a levelised cost of electricity comparable to traditional power plants [2]. Moreover, with the integration of Thermal Energy Storage (TES), CSP plants can operate in the absence of solar irradiation for continuous power generation, which would help mitigate the mismatch between peak electricity demand and solar energy production to ease the grid management challenges associated with the increased use of solar energy devices [3, 4]. These CSP plants, however, must operate reliably for up to 30 years, which poses a significant challenge due to the impact of harsh operational environment on the materials [5].

The next-generation CSP plant, as shown in Figure 1, contains three primary systems: a solar collector, Thermal Energy Storage (TES), and a power block with an expected peak temperature of up to 800 ℃ [6, 7]. Additionally, each of these systems relies on molten sodium as a Heat Transfer Fluid (HTF) to move heat from the solar tower to the TES and power block. The TES stores heat up to 750 ℃ through the use of a Phase Change Material (PCM) proposed to be a mixture of eutectic salt or the recently proposed aluminium [8]. The stored heat is transferred back to the HTF to deliver energy, for up to 8 hours [2, 9-11], to the power generation cycle in this case a supercritical CO_2 cycle at around 700 ℃ [2, 12, 13].
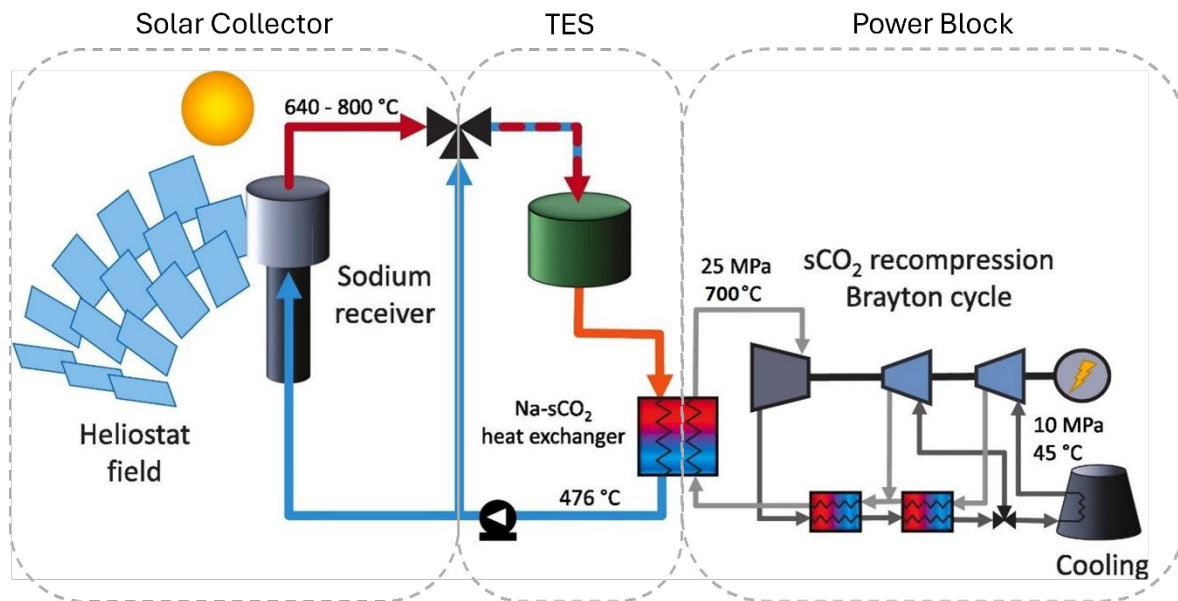

Figure 1. *Next-generation CSP plant schematic [2]*

The implementation of these novel technologies in CSP plants enhances efficiency, with early prototypes achieving a solar multiple in the range of 1.8 to 2.5, indicating sufficient excess power availability to fully utilise the TES system [7, 14]. However, the elevated temperature of the system, along with the corrosive operational environment, could initiate a multitude of failure modes in the material used to contain and convey the HTF, PCM and supercritical CO_2 within the power plant [15]. Hence, the scope of this study is limited to the study of the sodium loop in the CSP systems, where the primary mode of failure is expected to be Liquid Metal Embrittlement (LME) to avoid any potential catastrophic failures.

1.1 Liquid Metal Embrittlement (LME)

LME can result in increased susceptibility to brittle failure in normally ductile metals as a result of exposure to specific liquid metals. The mechanism governing this failure is highly variable and depends upon several factors, such as microstructure, temperature, stresses, and metal, among others [16]. This variability causes difficulties in determining the material susceptibility for LME, which requires extensive investigation of the operational environments [17]. The solar thermal power plant proposed for this research uses liquid sodium as HTF, which would interact with the base metals of the receiver, HTF pipes, and Heat Exchangers. The LME mechanism leads to degradation of ductility of the base metal and subsequent brittle failure. The increase in temperature accelerates crack initiation in certain alloys, along with selective leaching of base metals, leading to corrosion-type failure[18]. Serre [19] reported that T91 steel is susceptible to LME at 500 ℃ in liquid Lead Bismuth Eutectic (LBE). In contrast, Gong et al. [20] showed that the Fe10Cr4Al ferritic alloy has LME resistance above 450 ℃ in LBE, and the material regains ductility at 500 ℃, which reaffirms the belief that LME failure mechanisms are highly variable.

The LME process ordinarily has three steps similar to Stress Corrosion Cracking (SCC): exposure, penetration, and crack initiation/propagation. However, unlike SCC, crack initiation in LME is generally not driven by stresses. When tensile stresses are present, they can facilitate penetration, leading to grain boundary wetting and decohesion [16, 21]. Hence, while testing for LME vulnerability, specimens similar to an SCC test have traditionally been used to accelerate the tests [17, 22-24]. However, this method requires incubation time to test the material, which increases the time needed for the experimentation of each material. Thus, recent studies have adopted a Small Punch Test (SPT) methodology for experiments [25-29] that allows for a shorter test time along with a reduction in sample size, allowing controlled experiments with a reduced surface area with wetting by liquid metal while tensile stresses are externally applied. Moreover, the small sample size makes SPT a form of non-destructive test as samples can be extracted directly from an operational system and tested for integrity and remaining life assessment [30]. Hamdane [29] used the small punch test method for T91 steel at 450 ℃ in molten sodium and confirmed intergranular LME occurrence. Whereas Serre [26] conducted a comparative study of a set of austenitic, chromium, and Yttrium oxide (Y_2O_3) reinforced steels up to 550 ℃ in molten sodium using a small punch test. The study revealed the susceptibility of 14CrODS steel, whereas 316LN steel was found to fracture in fully ductile mode.

1.2 Research Significance

Numerous studies have been conducted to better understand LME occurrence in contact with liquid sodium with commercial alloys between 300 to 800 ℃, as LME affects are expected to be exacerbated by factors including, but not limited to, increased diffusion [31], reduced surface tension [25] and enhanced crack growth [18]. However, diurnal cyclic temperature variation commonly associated with CSP plants, along with operational breakdown, can result in plant temperature reducing below the known temperature range of LME interaction in the published literature. The current study aims to address this gap by conducting LME studies between 100 ℃ to 300 ℃ for 316L in contact with liquid sodium.

2. Methodology

2.1 Test Apparatus

The small punch test is a relatively novel method used for fracture mechanics testing of materials where it has been proposed to ease the testing process of material properties such as yield strength, creep, and ultimate tensile strength, among others, when only small amounts of material are available for experimentation. The test apparatus, as depicted in Figure 2, is modified from ASTM E3205 – 20 [32] and designed with the intent to hold liquid metal on the top of the small punch specimen, where the hemispherical punch with a 2.5 mm diameter was applied to the lower surface of the sample, allowing the top surface in contact with the liquid sodium to produce tensile stresses. Moreover, to reduce the exposure of liquid sodium to atmospheric air and humidity, the upper cavity is designed to be sealed with an inert gas. The set-up utilises a force transducer and extensometer to monitor the applied load and displacement until rupture, which enables LME detection as a result of reduced ductility of the test material [26]. Additionally, this allows in-situ testing with direct contact of the embrittling liquid with the material candidate, as the material properties are known to be reinstated upon removal of the liquid metal [18].
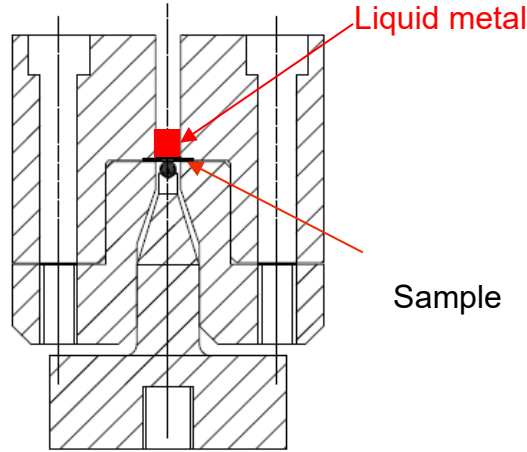
Figure 2. *Small Punch Test Apparatus for LME*

2.2 Test Specimen

The test specimen for experimental studies was manufactured in accordance with the ASTM standard E3205 – 20 [32]. The thin disk specimens used for experiments are manufactured from Brass and AISI 316L and 8 mm in diameter with a tolerance of ±0.01mm and 0.5 mm in thickness with a tolerance of ±0.005 mm. The specimens are manufactured by machining up to 1.2 times the thickness and ground on abrasive paper of P320 followed by P1200 grit size up to the required thickness to acquire the final specimens.

2.3 Experimental Strategy

The experimental tests were conducted using the standard process of testing the 316L specimen with and without liquid sodium to compare the impact of the corrosive environment by observing the change in fracture toughness. The methodology and test apparatus were verified using CZ121 brass embrittled by liquid galinstan, a gallium-indium-tin alloy that is known to embrittle brass [33]. Brass coated with liquid galinstan was tested at temperatures from 10 ℃ to 43 ℃ as the liquid metal is known to melt at -19 ℃. The test was repeated three times at each temperature interval to ensure consistent results, and the acquired load vs displacement plot was analysed to calculate the work of fracture given by equation 1 to examine the energy required to cause a fracture. The equation integrates applied force (F) with reference to the change in displacement ($d\delta$) to calculate the area under the load-displacement curve that defines work done in the system.

$$W = \int F \, d\delta \tag{1}$$

Once the validation study was successfully conducted, tests were repeated for 316L stainless steel using liquid sodium at 110 ℃, 150 ℃, and 300 ℃ in sets of 10 specimens per temperature interval for Na exposed condition and four without Na exposure. It is important to note that the stainless steel was polished and etched prior to tests, similar to the brass samples, to ensure the wetting of the alloy with sodium.

## 3. Results

3.1 Validation Study

The brass samples were tested at varying intervals between 10 ℃ and 43 ℃ and compared to tests performed both with and without Galinstan exposure. Figure 3 shows tests conducted

at the two extreme conditions of 10 ℃ and 43 ℃, with the plot showing force displacement acquired during the tests that are generally conducted until the rupture of the specimen. The analysis of this data should be a reasonable indication of LME, as evidenced by the significant reduction in force required to rupture the Galinstan exposed samples. However, this does not provide insights into how the materials deform, redistribute stress, and ultimately lead to fracture. Additionally, the force-displacement curve is highly variable based on the sample size, and the variability in the small SPT samples can lead to misinterpretation of results. Hence, this data is utilised to calculate a more reliable and comprehensive form of measurement referred to as work of fracture.
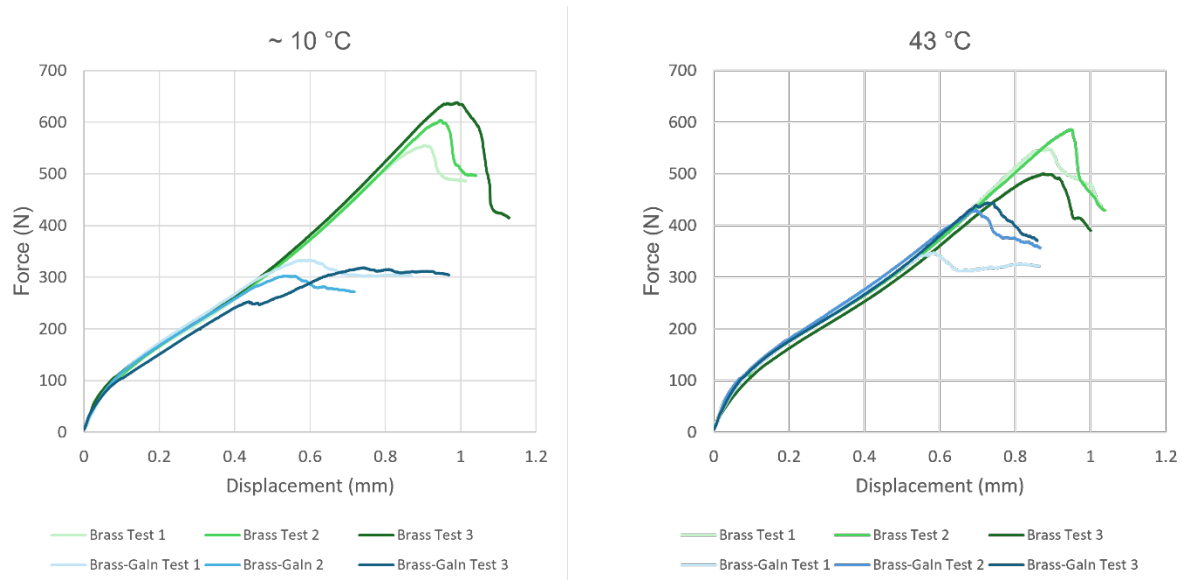
Figure 3. Force-displacement curve acquired from SPT conducted on CZ121 Brass with and without Galinstan Exposure

The work of fracture calculated from the force-displacement plots is displayed in Figure 4, where the x-axis shows the temperature of the test and the y-axis represents the work of fracture. The Galinstan exposed samples are depicted by black circular data points on the scatter plot, and the air-exposed samples are shown as hollow circles.
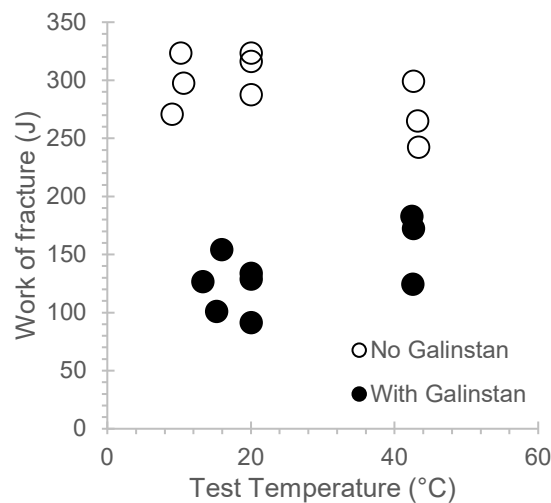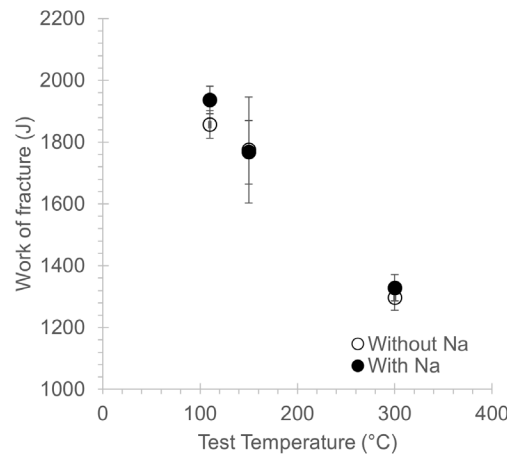

Figure 4. Work of fracture as a function of temperature acquired for CZ121 Brass with and without Galinstan Exposure

The tests conducted at and below the room temperature show the work of fracture at a consistently high value of up to 350 Joules, suggesting that the brass boasts a substantial

ability to resist fracture under standard temperature conditions in the air associated with ductile failure. Whereas, the Galinstan exposed samples show a significant effect on the material's toughness with reduced energy required to fracture at around 150 Joules. This suggests Brass-Galinstan LME occurrence leading to premature failure of the sample. While the failure occurs at both test temperatures, the 10 ℃ condition was noted to be most prominent compared to higher temperatures. This effect is believed to be caused by reduced ductility of the brass alloy at lower temperatures, which facilitates the brittle failure mode. The pilot experiments confirm that the test method is suitable for the intended purpose of the study of LME and can be used to conduct 316L-Na experiments.

3.2 Steel-Sodium Tests

The 316L alloy of interest was tested in contact with liquid sodium at 110 ℃, 150 ℃ and 300 ℃ with the SPT method, where the results acquired are depicted in Figure 5. The data from force-displacement curves were used to calculate the work of fracture, similar to the previous section. The tests were repeated 10 times for samples exposed to liquid sodium to account for LME variability and 4 times for air-exposed samples at each temperature. This data is represented as mean observed values in the figure with the error bars showing standard deviation between the tests.

Figure 5. Work of fracture as a function of temperature acquired for 316L with and without liquid sodium Exposure

The data shows a reduction in fracture toughness of 316L with temperature; however, there is no distinguishable difference in the samples exposed to sodium at any temperature. While this can be associated with difficulties in thoroughly wetting the 316L samples due to the passivity of the alloy, it does imply that the alloy retains its mechanical properties. Future studies with enhanced surface wetting techniques or different temperature conditions may provide additional insights, but the current data suggests that LME is not a critical factor for 316L at this temperature range.

4. Conclusion

The small punch test has the potential to be a useful screening test for materials susceptibility to LME and can be easily modified for testing at elevated temperatures. This research indicates that within the identified temperature range (100 - 300 ℃), 316L showed a low likelihood of LME induced by liquid sodium, which is consistent with other work carried out at higher temperatures. LME is primarily influenced by the interaction between liquid and solid metals, with passive films often acting as a barrier. Further work is needed to fully understand whether liquid sodium can penetrate the passive oxide layer on the stainless steel after long term exposure, such as in the case of solar thermal heat exchangers.

Data availability statement

The data used for the study can be made available upon reasonable request.

Author contributions

Stuart Bell: Conceptualisation, Methodology, Investigation, Resources, Formal analysis, Data Curation, Supervision. **Gaurav Vithalani**: Conceptualisation, Data Curation, Writing - Original Draft, Writing - Review & Editing. **Richard Clegg**: Methodology, Investigation, Resources, Formal analysis, Data Curation, Supervision, Writing - Review & Editing. **Geoffrey Will**: Conceptualisation, Methodology, Resources, Supervision, Funding acquisition, Writing - Review & Editing. **Theodore Steinberg**: Supervision, Funding acquisition, Writing - Review & Editing. **Rezwanul Haque**: Writing - Review & Editing.

Competing interests

The authors declare that they have no competing interests

Funding

References

[1]   N.K. Roy, A. Das, Prospects of Renewable Energy Sources, in: M.R. Islam, N.K. Roy, S. Rahman (Eds.) Renewable Energy and the Environment, Springer Singapore, Singapore, 2018, pp. 1-39.

[2]   A. de la Calle, A. Bayon, J. Pye, Techno-economic assessment of a high-efficiency, low-cost solar-thermal power system with sodium receiver, phase-change material storage, and supercritical CO_2 recompression Brayton cycle, Solar Energy, 199 (2020) 885-900.

[3]   I. Sarbu, C. Sebarchievici, A comprehensive review of thermal energy storage, Sustainability, 10 (2018) 191.

[4]   B. Bokelman, E.E. Michaelides, D.N. Michaelides, A Geothermal-Solar Hybrid Power Plant with Thermal Energy Storage, Energies (Basel), 13 (2020) 1018.

[5]   G. Vithalani, S. Bell, G. Will, T.A. Steinberg, R.E. Clegg, R. Haque, Investigation of Factors Affecting Corrosion Mechanisms in Latent Heat Thermal Energy Storage Systems, in: SolarPACES: International Conference on Concentrating Solar Power and Chemical Energy Systems, TIB Open Publishing.

[6]   J. Coventry, M. Arjomandi, C.-A. Asselineau, A. Chinnici, C. Corsi, D. Davis, J.-S. Kim, A. Kumar, W. Lipiński, W. Logie, Development of ASTRI high-temperature solar receivers, in: AIP Conference Proceedings, AIP Publishing LLC, 2017, pp. 030011.

[7]   M. Aghaeimeybodi, A. Beath, B. Webby, Techno-economic analysis of solar tower reference plant, in, CSIRO, Newcastle, NSW, Australia, Technical Report, https://astri.org.au, 2017.

[8]   M. Liu, S. Riahi, R. Jacob, M. Belusko, F. Bruno, Design of sensible and latent heat thermal energy storage systems for concentrated solar power plants: Thermal performance analysis, Renewable Energy, 151 (2020) 1286-1297.

[9]   A. de la Calle, A. Bayon, J. Hinkley, J. Pye, System-level simulation of a novel solar power tower plant based on a sodium receiver, PCM storage and sCO2 power block, in: AIP Conference Proceedings, AIP Publishing LLC, 2018, pp. 210003.

[10] M. Liu, W. Saman, F. Bruno, Review on storage materials and thermal performance enhancement techniques for high temperature phase change thermal storage systems, Renewable and Sustainable Energy Reviews, 16 (2012) 2118-2132.

[11] L. Qi, C. Lin, Z. Xusheng, D. Bo, Z. Boyang, D. Zheng, X. Yaxuan, L. Chuan, Fabrication and thermal properties investigation of aluminium based composite phase change material for medium and high temperature thermal energy storage, Solar Energy Materials & Solar Cells, 211 (2020) 162-171.

[12] A. Post, A. Beath, E. Sauret, R. Persky, Evaluation of power block arrangements for 100MW scale concentrated solar thermal power generation using top-down design, in: AIP Conference Proceedings, AIP Publishing LLC, 2017, pp. 030039.

[13] S. Bell, M.A. Rhamdhani, T. Steinberg, G. Will, Aggressive corrosion of C-276 nickel superalloy in chloride/sulphate eutectic salt, Solar Energy, 227 (2021) 557-567.

[14] J.-S. Kim, A. Kumar, C. Corsi, Design boundaries of large-scale falling particle receivers, in: AIP Conference Proceedings, AIP Publishing LLC, 2017, pp. 030029.

[15] G. Vithalani, S. Bell, G. Will, R. Clegg, T.A. Steinberg, R. Haque, Novel method for evaluation of stress assisted corrosion through compact tension specimens to assess material compatibility in latent heat thermal energy storage systems, Solar Energy Materials and Solar Cells, 266 (2024) 112658.

[16] D.G. Kolman, A review of recent advances in the understanding of liquid metal embrittlement, Corrosion, 75 (2019) 42-57.

[17] K. Sadananda, A.K. Vasudevan, Review of Environmentally Assisted Cracking, Metallurgical and materials transactions. A, Physical metallurgy and materials science, 42 (2011) 279-295.

[18] J. Norkett, M. Dickey, V. Miller, A Review of Liquid Metal Embrittlement: Cracking Open the Disparate Mechanisms, Metallurgical and Materials Transactions A, (2021) 1-15.

[19] I. Serre, J.-B. Vogt, Liquid metal embrittlement of T91 martensitic steel evidenced by small punch test, Nuclear engineering and design, 237 (2007) 677-685.

[20] X. Gong, F. Hu, J. Chen, H. Wang, H. Gong, J. Xiao, H. Wang, Y. Deng, B. Pang, X. Huang, Effect of temperature on liquid metal embrittlement susceptibility of an Fe10Cr4Al ferritic alloy in contact with stagnant lead-bismuth eutectic, Journal of Nuclear Materials, 537 (2020) 152196.

[21] H.-S. Nam, D.J. Srolovitz, Effect of material properties on liquid metal embrittlement in the Al–Ga system, Acta Materialia, 57 (2009) 1546-1553.

[22] L. Medina-Almazan, T. Auger, D. Gorse, Liquid metal embrittlement of an austenitic 316L type and a ferritic–martensitic T91 type steel by mercury, Journal of nuclear materials, 376 (2008) 312-316.

[23] D. Kolman, R. Chavarria, Liquid-metal embrittlement of type 316L stainless steel by gallium as measured by elastic-plastic fracture mechanics, Corrosion, 60 (2004).

[24] D. Kolman, R. Chavarria, Liquid-metal embrittlement of 7075 aluminum and 4340 steel compact tension specimens by gallium, Journal of testing and evaluation, 30 (2002) 452-456.

[25] I. Proriol Serre, J.-B. Vogt, Liquid metal embrittlement sensitivity of the T91 steel in lead, in bismuth and in lead-bismuth eutectic, Journal of Nuclear Materials, 531 (2020).

[26] I. Proriol Serre, O. Hamdane, J.-B. Vogt, Comparative study of the behavior of different highly alloyed steels in liquid sodium, Nuclear Engineering and Design, 320 (2017) 17-27.

[27] Y. Changqing, J.B. Vogt, I. Proriol Serre, Liquid metal embrittlement of the T91 steel in lead bismuth eutectic: the role of loading rate and of the oxygen content in the liquid metal, Materials Science and Engineering: A (Structural Materials: Properties, Microstructure and Processing), 608 (2014) 242-248.

[28] T. Auger, J.-B. Vogt, I.P. Serre, Liquid Metal Embrittlement, in: Mechanics-Microstructure-Corrosion Coupling, Elsevier, 2019, pp. 507-534.

[29] O. Hamdane, I. Proriol Serre, J.B. Vogt, N. Nuns, ToF-SIMS analyses of brittle crack initiation of T91 steel by liquid sodium, Materials Chemistry and Physics, 145 (2014) 243-249.

[30] S. Arunkumar, Overview of small punch test, Metals and Materials International, 26 (2020) 719-738.

[31] Y. Ikeda, R. Yuan, A. Chakraborty, H. Ghassemi-Armaki, J.M. Zuo, R. Maaß, Early stages of liquid-metal embrittlement in an advanced high-strength steel, Materials Today Advances, 13 (2022) 100196.

[32] A. E-20., Standard Test Method for Small Punch Testing of Metallic Materials, in, ASTM International West Conshohocken. PA, 2020.

[33] R. Clegg, Continuous and discontinuous crack growth in brass embrittled by liquid gallium, (2009).